# Geoelectrical fields in a layered earth with arbitrary anisotropy

Changchun Yin* and Peter Weidelt*

## ABSTRACT

In many cases in geoelectrical exploration, the standard model of a layered isotropic half-space is a good approximation to geophysical reality. But sometimes it is useful to extend this model to uniform anisotropic layers. For example, in regions with distinct dipping stratification, one will try to represent this conductivity variation in the form of dipping anisotropic layers. In this paper, the layered isotropic half-space is extended to a half-space with general anisotropy such that to each layer is assigned a symmetrical ($3 \times 3$) resistivity tensor.

After formulating the general layered problem, the numerical implementation is treated. A very fast algorithm exists only if the resistivity tensor is rotationally symmetric around a vertical axis (transverse isotropy). In all other cases, one has to calculate a double integral with respect to the horizontal components of the wavenumber vector. Furthermore, we have also calculated the magnetic field. Whereas in the isotropic case this field does not contain any information about the resitivity distribution, in the case of arbitrary anisotropy it carries some information about the distribution of resistivity inside the earth. No correct results are obtained if one interprets data resulting from an anisotropic structure by an isotropic model.

## INTRODUCTION

In the last few years, a great number of interpretation methods with variable isotropic electrical conductivity have been developed, but not enough attention has been paid to the effects of anisotropy, especially the arbitrary anisotropy of the earth. The effect of anisotropy on apparent resistivity was mentioned earlier in the geophysical literature by Slichter (1933) and Pirson (1935), but their research concentrated on the uniform transverse isotropic half-space only. In that case, the solution for the potential is usually obtained by replacing the anisotropic resistivity by an isotropic medium with the resistivity being the geometric mean of the vertical and radial resistivity. Also for the layered transverse isotropic earth, one can use the equivalent isotropic models to replace the anisotropic resistivity (Niwas and Upadhyaya, 1974; Pal and Das Gupta, 1984).

The model of a dipping anisotropic half-space is proposed for the first time by Bhattacharya and Patra (1968). The most advanced model considered so far is that of Gurevich (1975). It consists of a layered half-space with dipping anisotropy, the only restriction being that the horizontal strike direction is the same in all layers. Pal and Mukherjee (1986) calculated the electrical potential due to a point current source over a two-layer earth with a dipping anisotropic top layer. Negi and Saraf (1989) review the research on electrical anisotropy, which has been the subject of much attention in electrical prospecting (e.g., Kunz and Moran, 1958; Asten, 1974; Moran and Gianzero, 1979, 1982).

In this paper, the current density and magnetic field as source-free vectors are represented by poloidal and toroidal scalars. This representation has been applied by Maurer (1993) to model the problem of electric dipole induction in arbitrary anisotropic half-space. In the present direct current (dc) case, the system of differential equations leads to a simple stable recursive algorithm for both the electric and magnetic fields. For the latter, a Green's function approach is used.

## BASIC EQUATIONS

In dc prospecting, the electromagnetic fields $\mathbf{E}$, $\mathbf{H}$, $\mathbf{B}$ and the current density $\mathbf{J}$ satisfy the following equations:

$$\nabla \times \mathbf{E} = \mathbf{0}, \qquad \nabla \cdot \mathbf{J} = 0, \tag{1}$$

$$\nabla \times \mathbf{H} = \mathbf{J}, \qquad \nabla \cdot \mathbf{B} = 0, \tag{2}$$

where $\mathbf{J} = \underset{\sim}{\sigma}\mathbf{E} + \mathbf{J}_e$. Here $\mathbf{J}_e$ is the source current density and

$$\underset{\sim}{\sigma} = \underset{\sim}{\rho}^{-1}, \qquad \underset{\sim}{\rho} = \begin{pmatrix} \rho_{xx} & \rho_{xy} & \rho_{xz} \\ \rho_{xy} & \rho_{yy} & \rho_{yz} \\ \rho_{xz} & \rho_{yz} & \rho_{zz} \end{pmatrix} \tag{3}$$

are the conductivity and resistivity tensors, respectively. In the earth, these tensors are symmetric (Onsager, 1931) and positive-definite. The latter is required to ensure that the specific energy dissipation $\mathbf{E}\underset{\sim}{\sigma}\mathbf{E}$ is positive. In the air, we assume $\underset{\sim}{\sigma} = \underset{\sim}{\mathbf{0}}$. The magnetic permeability of the earth is assumed to be constant everywhere and equal to the vacuum permeability $\mu_0$.

Equations (1) and (2) show that the magnetic field $\mathbf{H} = \mathbf{B}/\mu_0$ and the current density $\mathbf{J}$ are solenoidal vector fields. Therefore, we can represent each of these fields by a toroidal and a poloidal scalar (Backus, 1958), i.e.,

$$\mathbf{H} = \nabla \times (\hat{\mathbf{z}} T_H) + \nabla \times \nabla \times (\hat{\mathbf{z}} P_H), \qquad (4)$$

$$\mathbf{J} = \nabla \times (\hat{\mathbf{z}} T_J) + \nabla \times \nabla \times (\hat{\mathbf{z}} P_J), \qquad (5)$$

where $\hat{\mathbf{z}}$ is a unit vector in vertical direction of the Cartesian coordinate system with the air-earth interface as origin of the $z$-coordinate. Since no currents flow in the insulating air half-space, $P_J = 0$ and $T_J = 0$ in $z < 0$. With the toroidal scalars are associated field lines closed in horizontal planes.

In the horizontal wavenumber domain $\mathbf{k} = u\hat{\mathbf{x}} + v\hat{\mathbf{y}}$, all fields are identified by a tilde and are connected with the corresponding fields in the space domain by

$$F(x, y) = \frac{1}{4\pi^2} \int_{-\infty}^{\infty} \int_{-\infty}^{\infty} \tilde{F}(u, v) \, e^{i(ux+vy)} \, du \, dv. \qquad (6)$$

Equations (5) and (4) yield as representation of the Cartesian components of $\tilde{\mathbf{J}}$ and $\tilde{\mathbf{H}}$

$$\tilde{\mathbf{J}} = \begin{pmatrix} iv\tilde{T}_J + iu\tilde{P}_J' \\ -iu\tilde{T}_J + iv\tilde{P}_J' \\ k^2\tilde{P}_J \end{pmatrix}, \qquad \tilde{\mathbf{H}} = \begin{pmatrix} iv\tilde{T}_H + iu\tilde{P}_H' \\ -iu\tilde{T}_H + iv\tilde{P}_H' \\ k^2\tilde{P}_H \end{pmatrix}, \qquad (7)$$

where $k := |\mathbf{k}|$ and the prime denotes differentiation with respect to $z$. From

$$\hat{\mathbf{z}} \cdot (\nabla \times \mathbf{H} - \mathbf{J}) = 0 \quad \text{and} \quad \hat{\mathbf{z}} \cdot \nabla \times (\nabla \times \mathbf{H} - \mathbf{J}) = 0 \quad (8)$$

follows $T_H = P_J$ and $T_J = -\nabla^2 P_H$, and therefore

$$\tilde{T}_H = \tilde{P}_J, \qquad \tilde{T}_J = k^2\tilde{P}_H - \tilde{P}_H''. \qquad (9)$$

The first equation expresses the well-known result that toroidal magnetic fields are confined to conductors. Furthermore,

$$\hat{\mathbf{z}} \cdot \nabla \times \mathbf{E} = \hat{\mathbf{z}} \cdot \nabla \times (\underset{\sim}{\rho}\mathbf{J}) = 0 \quad \text{and}$$

$$\hat{\mathbf{z}} \cdot \nabla \times \nabla \times \mathbf{E} = \hat{\mathbf{z}} \cdot \nabla \times \nabla \times (\underset{\sim}{\rho}\mathbf{J}) = 0 \qquad (10)$$

yield on account of equation (9) within uniform layers

$$d\tilde{P}_J'' + 2e\tilde{P}_J' - (c^2 + af)\tilde{P}_J = 0, \qquad (11)$$

$$-\tilde{P}_H'' + k^2\tilde{P}_H = (ck^2\tilde{P}_J - b\tilde{P}_J')/a = \tilde{T}_J, \qquad (12)$$

where

$$a := v^2\rho_{xx} - 2uv\rho_{xy} + u^2\rho_{yy}, \qquad (13)$$

$$b := (v^2 - u^2)\rho_{xy} + uv(\rho_{xx} - \rho_{yy}), \qquad (14)$$

$$c := iv\rho_{xz} - iu\rho_{yz}, \qquad (15)$$

$$d := \rho_{xx}\rho_{yy} - \rho_{xy}^2, \qquad (16)$$

$$e := iv(\rho_{xz}\rho_{xy} - \rho_{yz}\rho_{xx}) + iu(\rho_{yz}\rho_{xy} - \rho_{xz}\rho_{yy}), \quad (17)$$

$$f := \rho_{zz}. \qquad (18)$$

At internal layer boundaries, the vector $\mathbf{H}$, the normal component of $\mathbf{J}$, and the tangential component of $\mathbf{E}$ are continuous. This implies

$$[\tilde{P}_H] = 0, \qquad [\tilde{P}_H'] = 0, \qquad [\tilde{P}_J] = 0,$$

$$[(d\tilde{P}_J' + e\tilde{P}_J)/a] = 0, \qquad (19)$$

where $[\,]$ means the jump of the function across the boundary. The last condition is obtained as follows (Maurer, 1993): Since $\mathbf{E}$ is a potential field, $\hat{\mathbf{z}} \cdot (\mathbf{k} \times \tilde{\mathbf{E}}) = 0$ is identically satisfied. The tangential electric field is therefore continuous if we impose the additional condition $[\mathbf{k} \cdot \tilde{\mathbf{E}}] = 0$, which then provides the fourth continuity condition after eliminating in equation (7) $\tilde{T}_J$ by $\tilde{P}_J$ on using equation (12).

The current sources, assumed at $z = 0$, are incorporated by the jump conditions (see Appendix A)

$$[\tilde{P}_J]_-^+ = \tilde{P}_J(0^+) =: D_J, \qquad (20)$$

$$[\tilde{P}_H']_-^+ = \tilde{P}_H'(0^+) - \tilde{P}_H'(0^-) = \tilde{P}_H'(0^+) - k\tilde{P}_H(0) =: D_H, \qquad (21)$$

where $[\varphi]_-^+ := \varphi(0^+) - \varphi(0^-)$. Assuming that there are two point sources feeding the current $+I$ at $\mathbf{r}_A = (x_A, y_A, 0)$ and $-I$ at $\mathbf{r}_B = (x_B, y_B, 0)$, we obtain with $\mathbf{r}_A - \mathbf{r}_B =: \hat{\mathbf{d}}|\mathbf{r}_A - \mathbf{r}_B|$ [see equations (A-4) and (A-10) in Appendix A]

$$D_J = \frac{I}{k^2}\{e^{-i\mathbf{k}\cdot\mathbf{r}_A} - e^{-i\mathbf{k}\cdot\mathbf{r}_B}\}, \qquad (22)$$

$$D_H = \begin{cases} +\dfrac{I}{k^2}\dfrac{\mathbf{k}\cdot(\hat{\mathbf{d}}\times\hat{\mathbf{z}})}{\mathbf{k}\cdot\hat{\mathbf{d}}}\{e^{-i\mathbf{k}\cdot\mathbf{r}_A} - e^{-i\mathbf{k}\cdot\mathbf{r}_B}\}, \\ \hspace{5cm} \mathbf{k}\cdot\hat{\mathbf{d}} \neq 0 \\ -\dfrac{I}{k^2}|\mathbf{r}_A - \mathbf{r}_B|i\mathbf{k}\cdot(\hat{\mathbf{d}}\times\hat{\mathbf{z}}) e^{-i\mathbf{k}\cdot(\mathbf{r}_A + \mathbf{r}_B)/2}, \\ \hspace{5cm} \mathbf{k}\cdot\hat{\mathbf{d}} = 0 \end{cases} \qquad (23)$$

If we are interested only in the electric fields and currents, we can confine our attention to the scalar $\tilde{P}_J$ as solution of equation (11), taking into account the source term (20) and the last two continuity equations of (19). The computational load is then comparable with that arising from the use of the electric scalar potential, which would be a good alternative choice in this case. However, if we are interested in addition in magnetometric resistivity studies (e.g. Edwards and Nabighian, 1991), the scalar $\tilde{P}_J$ gives, by using equations (12) and (21), an easy access to the magnetic scalar $\tilde{P}_H$, which describes the magnetic field in $z \leq 0$.

The most time-consuming part of the computation is the transformation from the wavenumber into the space domain, because it requires in general a double Fourier transform. Only in the simple case of transverse isotropy, where the transformed

field of a point source depends on $k^2 = u^2 + v^2$, it is then rotationally symmetric and we may resort to the fast Hankel transform techniques (e.g., Johansen and Sørensen, 1979).

## COMPUTATION OF $\tilde{P}_J(\mathbf{k}, z)$ AND $\tilde{P}_H(\mathbf{k}, z)$

We consider an earth consisting of $L$ uniform anisotropic layers. To layer $\ell$ with top at $z_\ell$ is assigned the resistivity tensor $\boldsymbol{\rho}_\ell, \ell = 1, \ldots, L$. Let $z_1 = 0$ and let $h_\ell := z_{\ell+1} - z_\ell$, $\ell = 1, \ldots, L - 1$ denote the layer thicknesses. The basic scalar $\tilde{P}_J$ is a solution of equation (11) with the source term (20), at layer boundaries subjected to the last two continuity conditions of equation (19). In each layer the solutions of equation (11) are exponential: $\tilde{P}_J(z) \sim \exp(-\alpha_\ell z)$. Insertion into equation (11) yields

$$d_\ell \alpha_\ell^2 - 2e_\ell \alpha_\ell - c_\ell^2 - a_\ell f_\ell = 0 \qquad (24)$$

or

$$\alpha_\ell^\pm = \beta_\ell \pm \gamma_\ell \qquad (25)$$

with

$$\beta_\ell := e_\ell/d_\ell,$$
$$\gamma_\ell := \sqrt{(c_\ell^2 + a_\ell f_\ell)d_\ell + e_\ell^2}/d_\ell = \sqrt{a_\ell \det \boldsymbol{\rho}_\ell}/d_\ell, \qquad (26)$$

where $\det \boldsymbol{\rho}_\ell$ is the determinant of the resistivity tensor in layer $\ell$. Since $\boldsymbol{\rho}_\ell$ has to be positive-definite, this determinant is positive. It also implies that $d_\ell > 0$. From equations (13) and (16) then follows

$$a_\ell \geq v^2 \rho_{xx} - 2|uv|\sqrt{\rho_{xx}\rho_{yy}} + u^2 \rho_{yy}$$
$$= (|v|\sqrt{\rho_{xx}} - |u|\sqrt{\rho_{yy}})^2 > 0, \qquad k > 0. \quad (27)$$

Therefore $\gamma_\ell > 0$ for $k > 0$. The quantity $\beta_\ell$ is purely imaginary and can have both signs. The complete solution of $\tilde{P}_J$ in layer $\ell$ is

$$\tilde{P}_J(z) = A_\ell^+ e^{-\alpha_\ell^+(z-z_\ell)} + A_\ell^- e^{-\alpha_\ell^-(z-z_\ell)}, \quad z_\ell < z < z_{\ell+1}. \qquad (28)$$

The superscript $+(-)$ denotes downgoing (upgoing) waves. Therefore $A_L^- = 0$. The application of the last two continuity equations of equation (19) at $z = z_{\ell+1}$ yields

$$A_\ell^+ e^{-\alpha_\ell^+ h_\ell} + A_\ell^- e^{-\alpha_\ell^- h_\ell} = A_{\ell+1}^+ + A_{\ell+1}^-, \qquad (29)$$

$$\xi_\ell(A_\ell^+ e^{-\alpha_\ell^+ h_\ell} - A_\ell^- e^{-\alpha_\ell^- h_\ell}) = \xi_{\ell+1}(A_{\ell+1}^+ - A_{\ell+1}^-), \quad (30)$$

with

$$\xi_\ell := \sqrt{\det \boldsymbol{\rho}_\ell/a_\ell}. \qquad (31)$$

Moreover let

$$B_\ell := \xi_\ell \frac{A_\ell^+ - A_\ell^-}{A_\ell^+ + A_\ell^-}. \qquad (32)$$

Expressing both $B_\ell$ and $B_{\ell+1}$ [via the ratio of equations (30)/(29)] in terms of the reflection coefficient $A_\ell^-/A_\ell^+$ and elim-

inating the latter, we obtain the recurrence relation

$$B_\ell = \xi_\ell \frac{B_{\ell+1} + \xi_\ell \tanh(\gamma_\ell h_\ell)}{\xi_\ell + B_{\ell+1} \tanh(\gamma_\ell h_\ell)}, \quad \ell = L - 1, \ldots, 1, \quad (33)$$

starting with $B_L = \xi_L$. The surface field is then obtained from $B_1$ and equation (20) (i.e., $A_1^+ + A_1^- = D_J$), yielding

$$A_1^+ = \frac{\xi_1 + B_1}{2\xi_1} D_J, \qquad A_1^- = \frac{\xi_1 - B_1}{2\xi_1} D_J, \quad \text{and}$$
$$\tilde{P}_J'(0^+) = -(\beta_1 + \gamma_1 B_1/\xi_1)D_J. \qquad (34)$$

The amplitudes $A_\ell^\pm, \ell > 1$, are recursively obtained from equations (29) and (30). Therefore, $\tilde{P}_J(z)$ can be assumed to be known. Stable computational methods are given in Appendix B.

For the computation of the magnetic field, we have to solve equation (12) with the source term (21). The magnetic field vanishes for $z \to \pm\infty$. Therefore let $G(z|z_0)$ be the full-space Green's function

$$G(z \mid z_0) = \frac{e^{-k|z-z_0|}}{2k} \qquad (35)$$

satisfying

$$G''(z \mid z_0) - k^2 G(z \mid z_0) = -\delta(z - z_0). \qquad (36)$$

Multiplication of equation (36) with $\tilde{P}_H(z)$ and of equation (12) with $G$ and integration of the difference over $z$ between 0 and $\infty$ yields after integration by parts on using equation (21)

$$2k\tilde{P}_H(z_0) = \int_0^\infty \tilde{T}_J(z) e^{-k|z-z_0|} dz - D_H e^{-k|z_0|}, \quad (37)$$

which holds both in the conductor $z_0 \geq 0$ and in the air half-space $z_0 < 0$. On the surface, we have

$$2k\tilde{P}_H(0) = \int_0^\infty \tilde{T}_J(z) e^{-kz} dz - D_H, \qquad (38)$$

$$2\tilde{P}_H'(0^+) = \int_0^\infty \tilde{T}_J(z) e^{-kz} dz + D_H. \qquad (39)$$

With a knowledge of $\tilde{P}_J(0^+)$, $\tilde{P}_J'(0^+)$, $\tilde{P}_H(0)$, and $\tilde{P}_H'(0^+)$, the components of $\tilde{\mathbf{J}}$ and $\hat{\mathbf{H}}$ at the surface of the earth are expressed as

$$\tilde{J}_x(0^+) = i[+vc_1 k^2 \tilde{P}_J(0^+) + (ua_1 - vb_1)\tilde{P}_J'(0^+)]/a_1, \qquad (40)$$

$$\tilde{J}_y(0^+) = i[-uc_1 k^2 \tilde{P}_J(0^+) + (va_1 + ub_1)\tilde{P}_J'(0^+)]/a_1, \qquad (41)$$

$$\tilde{J}_z(0^+) = k^2 \tilde{P}_J(0^+), \qquad (42)$$

$$\tilde{H}_x(0^+) = +iv\tilde{P}_J(0^+) + iu\tilde{P}_H'(0^+), \qquad (43)$$
$$\tilde{H}_x(0^-) = iuk\tilde{P}_H(0),$$

$$\tilde{H}_y(0^+) = -iu\tilde{P}_J(0^+) + iv\tilde{P}_H'(0^+),$$

$$\tilde{H}_y(0^-) = ivk\tilde{P}_H(0), \tag{44}$$

$$\tilde{H}_z(0) = k^2\tilde{P}_H(0), \tag{45}$$

where $a_1$, $b_1$, and $c_1$ are defined in equations (13)–(15). In the space domain, the discontinuity of $J_z$ is confined to the source points, and only the horizontal magnetic field in direction $\hat{\mathbf{d}} \times \hat{\mathbf{z}}$ is discontinuous across the straight cable connecting these points.

In the present approach, the vectors **J** and **H** are decomposed into toroidal and poloidal modes. Inside the conductor, the dominant poloidal current flow $P_J$ is associated with a toroidal magnetic field. Because of $T_H = P_J$, the toroidal magnetic field is absent in the air half-space. In the air, only the poloidal magnetic scalar $P_H$ exists. For isotropic or transverse isotropic layering where, according to equations (14), (15), and (12), $b \equiv 0$, $c \equiv 0$, and $\tilde{T}_J \equiv 0$, equation (37) yields

$$\tilde{P}_H(z) = -D_H\exp(-k|z|)/(2k), \tag{46}$$

such that in this case the magnetic field in the air half-space does not contain any information about the electrical structure. In the space domain, $P_H$ represents for $z < 0$ the magnetic field of the linear circuit consisting of the cable connecting $\mathbf{r}_B$ with $\mathbf{r}_A$, completed in the earth by two semi-infinite line currents flowing downwards at $\mathbf{r}_A$ and upwards at $\mathbf{r}_B$. However, azimuthal anisotropy ($b \not\equiv 0$) and/or dipping anisotropy ($c \not\equiv 0$) is associated with toroidal current flow ($\tilde{T}_J \not\equiv 0$), and therefore the magnetic field in the air contains, according to equation (37), some weak information about the electrical structure. This facet is discussed in detail by Edwards and Nabighian (1991) using a different approach.

### NUMERICAL RESULTS

#### Anisotropy paradox

As examples, we are considering only the results for a Schlumberger array. The first model is a dipping anisotropic half-space (see Figure 1). The longitudinal resistivity in the $\zeta$ and $\eta$ directions are $\rho_{\zeta\zeta} = \rho_{\eta\eta} = \rho_\ell = 25\,\Omega$m, the transverse resistivity in the $\xi$ direction is $\rho_{\xi\xi} = \rho_t = 100\,\Omega$m, the geometric mean of $\rho_\ell$ and $\rho_t$ is $\rho_m = \sqrt{\rho_\ell\rho_t} = 50\,\Omega$m, the dip of the stratification is $\alpha$. Figure 2 shows a polar representation of the comparison between the theoretical (Parasnis, 1986) and the computed anisotropy paradox on the surface of the earth for various dip angles $\alpha$. The length of the radius vector from the origin to each point gives the apparent resistivity and the direction of the radius vector defines the direction of the Schlumberger array. From Figure 2, one can see that (1) the computed and theoretical results agree, (2) for $\alpha = 0°$ the apparent resistivity for all directions is $\rho_a = \rho_m$, and (3) for $\alpha = 90°$, one measures along the strike (in the $y$-direction) the great apparent resistivity $\rho_a = \rho_m$, and perpendicular direction to the strike (in the $x$-direction) the small apparent resistivity $\rho_a = \rho_\ell$.

Figure 3 shows a two-layer model in which an anisotropic top layer with $\rho_{t1} = \rho_{\xi\xi1} = 100\,\Omega$m, $\rho_{\ell1} = \rho_{\zeta\zeta1} = \rho_{\eta\eta1} = 25\,\Omega$m,

$\rho_{m1} = \sqrt{\rho_{\ell1}\rho_{t1}} = 50\,\Omega$m, $h_1 = 100$ m, and $\alpha = 90°$ is located over an isotropic half-space with $\rho_2 = 120\,\Omega$m. Figure 4 shows that for small distances between a current source and measuring points the anisotropy paradox is very similar to that of an anisotropic half-space. With increasing distance, the apparent resistivity increases due to the high resistivity of the isotropic half-space, but the influence of the anisotropy of the first layer persists.

### Distribution of electric and magnetic fields

As pointed out in a previous section, the magnetic field on the surface of an isotropic or transverse isotropic layered earth
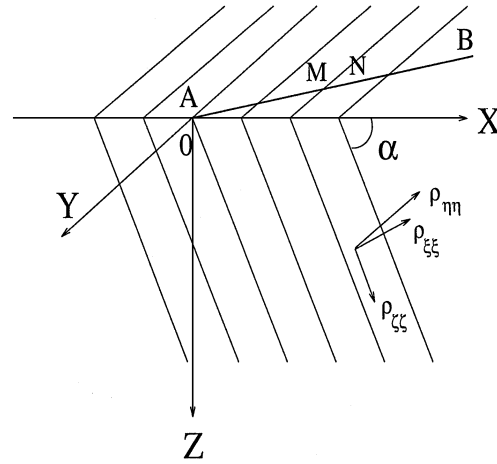


FIG. 1. Half-space with dipping anisotropy: $\rho_{\eta\eta}$, $\rho_{\zeta\zeta}$ are the longitudinal resistivities, $\rho_{\xi\xi}$ is the transverse resistivity, $\alpha$ is the dip of the stratification; A, B and M, N are, respectively, current and potential electrodes of the Schlumberger array.
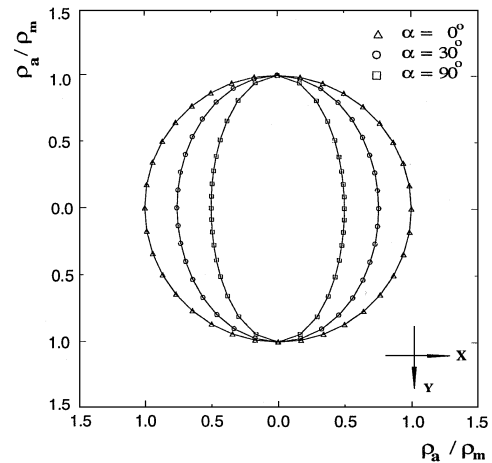


FIG. 2. Comparison of theoretical and computed anisotropy paradox for the dipping anisotropic half-space shown in Figure 1. $\rho_m$ is the geometric mean of the longitudinal and transverse resistivity; X, Y are the axes of the coordinate system shown in Figure 1, lines and symbols represent the theoretical and computed anisotropy paradox, respectively. Note that the distribution of apparent resistivity is different from that of real resistivity of the earth, which is the anisotropy paradox.

contains no information about the distribution of resistivity in the earth. However, azimuthal or dipping anisotropy is reflected in the magnetic field. Figure 5 shows the electric and the magnetic fields and the current density in the center between two electrodes A and B on the surface of an isotropic or a transverse isotropic half-space for different directions of the electrode array. The fields are radially symmetric. However, if the earth has azimuthal anisotropy (e.g., the model of Figure 1 with $\alpha = 90°$), then the current still flows in the radial direction and the magnetic field is tangential, but the magnitude of the fields changes with azimuth. The electric field is no longer radial, and its magnitude changes as well with azimuth (see Figure 6).

On the surface of a two-layer model with an anisotropic top layer located over an isotropic half-space (Figure 3), the influence of the deep isotropic half-space is barely visible for small distances between current source and measuring point; the distribution of fields is very similar to that above an anisotropic half-space. But with increasing distance, the distribution of the fields approaches that above an isotropic half-space except for current density, because the measuring points are located in the anisotropic top layer (see Figure 7).



FIG. 3. A two-layer earth with an anisotropic top layer. The thickness of the top layer is $h_1$, $\rho_2$ is the resistivity of isotropic half-space, the other parameters have the same meaning as in Figure 1.

## EFFECT OF ANISOTROPY ON THE GEOELECTRICAL INTERPRETATION

Maillet (1947) has established the basic equivalence that a transverse isotropic layer with longitudinal resistivity $\rho_\ell$, transverse resistivity $\rho_t$, and thickness $h$ cannot be distinguished by surface measurements from an isotropic layer with resistivity $\rho_{iso} = \sqrt{\rho_t \rho_\ell}$ and thickness $h_{iso} = h\sqrt{\rho_t/\rho_\ell} \geq h$, the invariants being the longitudinal conductance $h/\rho_\ell = h_{iso}/\rho_{iso}$ and the integrated transverse resistivity $h\rho_t = h_{iso} \cdot \rho_{iso}$.

Due to the anisotropy paradox, also the interpretation of data with azimuthal anisotropy by isotropic models will lead to erroneous results. This is exemplified by Schlumberger sounding data from the two-layer model with an anisotropic top layer as shown in Figure 3. The inversion is carried out with the Marquardt method. Figure 8 displays both the theoretical resistivity curves for this model with arrays (a) perpendicular and (b) parallel to the strike direction and the curves resulting from the isotropic models (given as inserts). The interpretation of the array perpendicular to the strike is dominated by the anisotropy paradox and the array parallel to the strike reveals $\sqrt{\rho_{\xi\xi 1} \cdot \rho_{\zeta\zeta 1}}$. In both cases the thickness of the top layer is underestimated. Apart from the fact that the inversion results depend on the alignment of the array, we also conclude from Figure 8 that the isotropic three-layer model fits the anisotropic data better than an isotropic two-layer model. This means that the anisotropy of the earth has rendered the resistivity profiles more complex.

## CONCLUSIONS

Using a field representation of the current density and the magnetic field in terms of poloidal and toroidal scalars, we give a unified treatment of the calculation of electric and magnetic dc fields in a layered conductor with an arbitrary anisotropic resistivity distribution. The problem is reduced to the determination of the scalar describing the poloidal current flow. It plays a similar rôle as the scalar electric potential would have played in an alternative formulation. However, the present approach also gives immediate access to the magnetic field. It is cast into a form that is numerically stable. As first applications, we revisit the well-known anisotropy paradox and present **E**, **J**, and **H** at the surface of an anisotropic earth. We also show that a perfect fit with erroneous results can be obtained when data originating from an anisotropic earth are interpreted in terms of an isotropic layered conductor. If the consideration of different array alignments reveals the anisotropy, this finding has to be taken into account in an adquate inversion procedure.
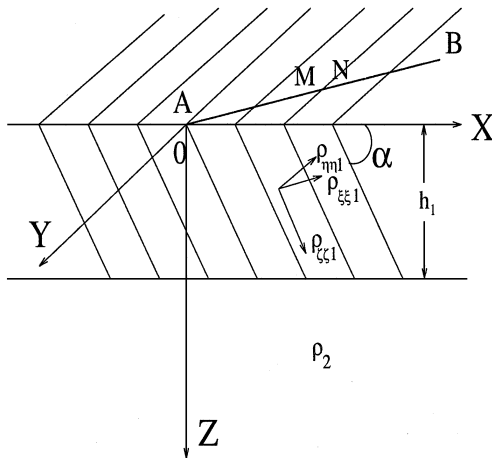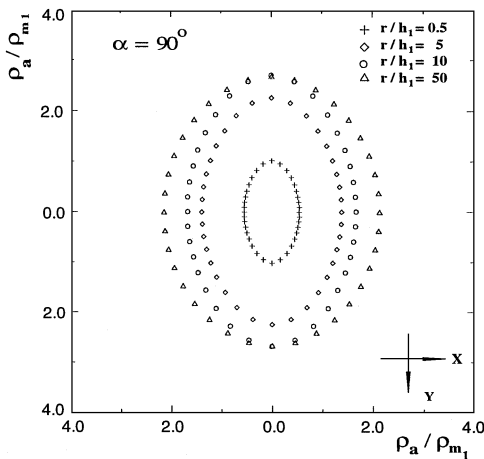


FIG. 4. Anisotropy paradox for the two-layer model shown in Figure 3. The dip of the stratification is $\alpha = 90°$, the parameters on the top right are the ratios of the half-distance between current electrodes and the thickness of the top layer. The apparent resistivity changes with the distance between current electrodes, but the influence of the anisotropy of the top layer persists.
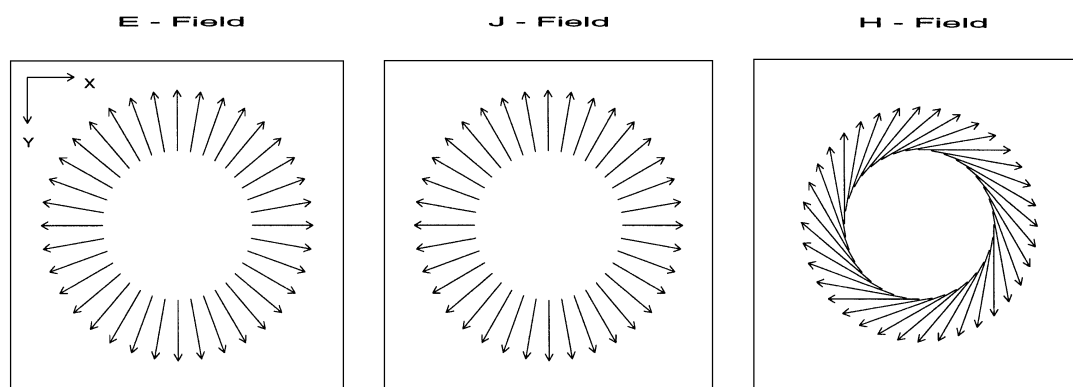
E - Field  J - Field  H - Field

FIG. 5. Distribution of electric field, current density, and magnetic field on the surface of an isotropic or a transverse isotropic half-space. The fields are calculated in the center between two current electrodes A and B for different directions of the Schlumberger array and normalized by the field in the *y*-direction. The starting point of each arrow is the measuring point; the length and direction of the arrow reflect the magnitude and the direction of the field at that point. X and Y are the axes of the coordinate system shown in Figure 1. One cannot distinguish between an isotropic and a transverse isotropic earth from the distribution of the electric field or the magnetic field.
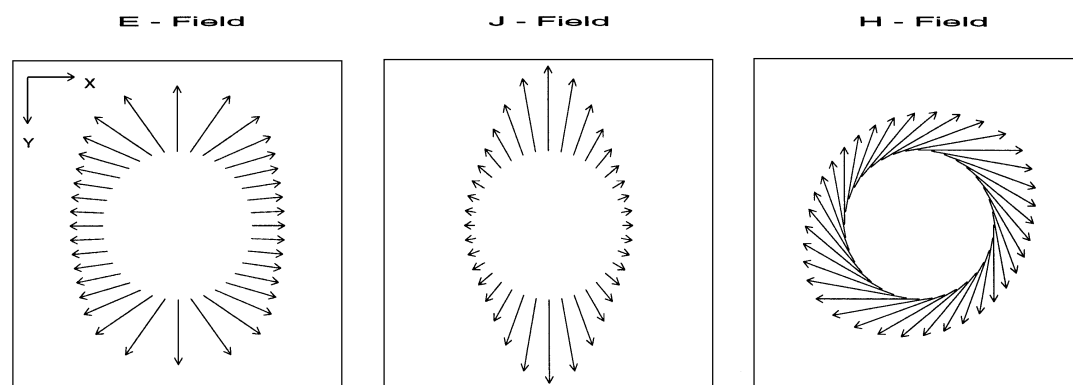
E - Field  J - Field  H - Field

FIG. 6. Distribution of electric field, current density, and magnetic field on the surface of an azimuthal anisotropic half-space shown in Figure 1 ($\alpha = 90°$). The distribution of both the electric and magnetic field reflects the character of the resistivity in the earth.

## REFERENCES

Asten, M. W., 1974, The influence of electrical anisotropy on mise-à-la-masse surveys: Geophys. Prosp., **22**, 238–245.
Backus, G. E., 1958, A class of self sustaining dissipative spherical dynamos: Ann. Phys., **4**, 372–447.
Bhattacharya, P. K., and Patra, H. P., 1968, Direct current geoelectrical sounding: Elsevier Publ. Co.
Edwards, R. N., and Nabighian, M. N., 1991, The magnetometric resistivity method, *in* Nabighian, M. N., Ed., Electromagnetic methods in applied geophysics, **2A**: Soc. Expl. Geophys., 47–99.
Gurevich, J. M., 1975, On theory of vertical electrical sounding for anisotropic media: Physics of the Earth (in Russian), **7**, 102–105.
Johansen, K., and Sørensen, K., 1979, Fast Hankel transforms: Geophys. Prosp., **27**, 876–901.
Kunz, K. S., and Moran, J. H., 1958, Some effects of formation anisotropy on resistivity measurements in boreholes: Geophysics, **23**, 770–794.
Maillet, R., 1947, The fundamental equations of electrical prospecting: Geophysics, **12**, 529–556.
Maurer, H.-M., 1993, Elektromagnetische Induktion in anisotropen Leitern: Ph.D. Thesis, Technical Univ. of Braunscheig.
Moran, J. H., and Gianzero, S., 1979, Effects of formation anisotropy on resistivity logging measurements: Geophysics, **44**, 1266–1286.
———1982, Electrical anisotropy, its effect on well logs, *in* Fitch, A. A., Ed., Developments in geophysical exploration: Applied Science Publ. Ltd., 195–238.
Negi, J. G., and Saraf, P. D., 1989, Anisotropy in geoelectromagnetism: Elsevier Publ. Co.
Niwas, S., and Upadhyaya, S. K., 1974, Theoretical resistivity sounding results over a transition layer model: Geophys. Prosp., **22**, 279–296.
Onsager, L., 1931, Reciprocal relations in irreversible processes: Phys. Rev., **37**, 405–426.
Pal, B. P., and Das Gupta, S. P., 1984, Electric potential due to a point current source over an inhomogeneous anisotropic earth: Geophys. Prosp., **32**, 943–954.
Pal, B. P., and Mukherjee, K., 1986, Electric potential due to a point current source over a layered conducting earth with dipping anisotropy: Geoexploration, **24**, 15–19.
Parasnis, D. S., 1986, Principles of applied geophysics (3rd edition): Chapman and Hall.
Pirson, S. J., 1935, Effect of anisotropy on apparent resistivity curves: AAPG Bull., **19**, 37–57.
Slichter, L., 1933, The interpretation of resistivity prospecting method for horizontal structures: Physics, **4**, 307–322.
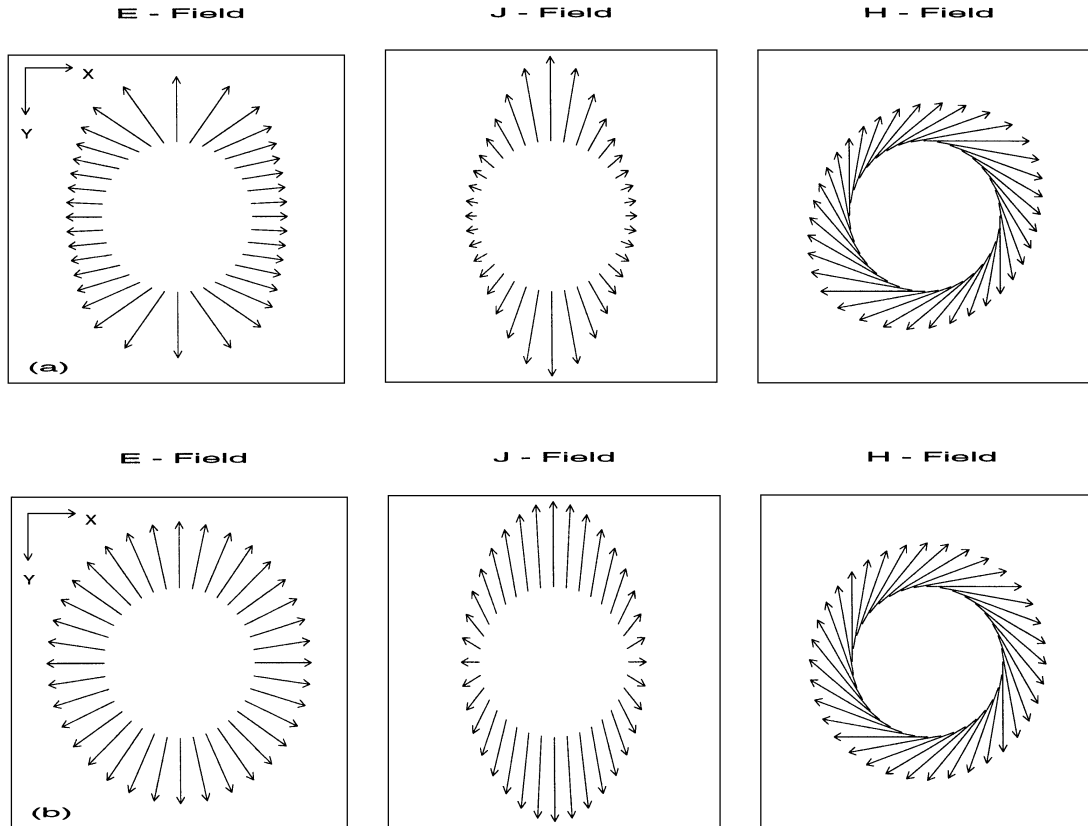
FIG. 7. Distribution of electric field, current density, and magnetic field on the surface of an anisotropic two-layer earth shown in Figure 3 ($\alpha = 90°$). The ratios of the half-distance between current electrodes and the thickness of the top layer are (a) $r/h_1 = 0.5$, (b) $r/h_1 = 80$. The distribution of fields changes with the separation between current electrodes: For the small separation (a), the fields resemble those of the anisotropic half-space of Figure 6, for the large separation (b), the underlying isotropic half-space induces via the continuity conditions almost isotropic horizontal electric and magnetic fields. Therefore, the anisotropy is mainly visible in the current density.
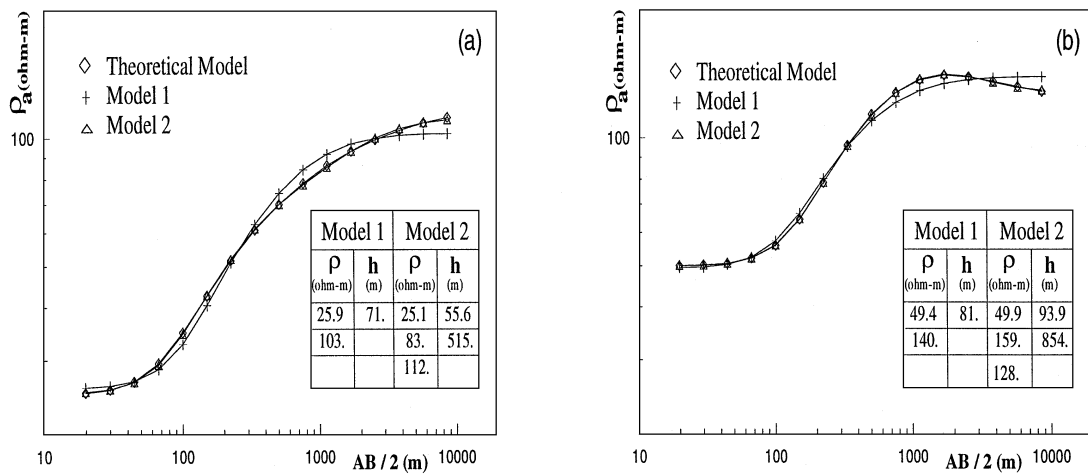


FIG. 8. Interpretation of Schlumberger data from a conductivity structure with azimuthal anisotropy in the top layer (Figure 3 with $\rho_{\xi\xi1} = 100\,\Omega\text{m}$, $\rho_{\zeta\zeta1} = \rho_{\eta\eta1} = 25\,\Omega\text{m}$, $h_1 = 100\,\text{m}$, $\alpha = 90°$, and $\rho_2 = 120\,\Omega\text{m}$) using an isotropic layered model. (a) Array aligned perpendicular to the strike direction; (b) array aligned parallel to the strike direction. The resulting inverse models are model 1 (two layers) and model 2 (three layers), given as inserts. Due to the anisotropy paradox, the isotropic interpretation is grossly in error.

## APPENDIX A

### COUPLING THE SOURCES

We assume that there are two point sources feeding the current $+I$ at $\mathbf{r}_A = (x_A, y_A, 0)$ and $-I$ at $\mathbf{r}_B = (x_B, y_B, 0)$. Then, $\mathbf{J} = \underline{\sigma}\mathbf{E}$ has the divergence

$$\nabla \cdot \mathbf{J} = I\{\delta_2(\mathbf{r} - \mathbf{r}_A) - \delta_2(\mathbf{r} - \mathbf{r}_B)\}\delta(z), \qquad \text{(A-1)}$$

where $\delta_2(\cdot)$ is the Dirac $\delta$ function in the $(x, y)$-plane. Integration over $z$ from $z = 0^-$ to $0^+$ yields, with $\mathbf{J}(z = 0^-) = \mathbf{0}$,

$$J_z(z = 0^+) = I\{\delta_2(\mathbf{r} - \mathbf{r}_A) - \delta_2(\mathbf{r} - \mathbf{r}_B)\}. \qquad \text{(A-2)}$$

The 2-D Fourier transformation of $J_z$ is

$$\tilde{J}_z(\mathbf{k}, 0^+) = I\{e^{-i\mathbf{k}\cdot\mathbf{r}_A} - e^{-i\mathbf{k}\cdot\mathbf{r}_B}\}. \qquad \text{(A-3)}$$

It then follows from equations (7) and (20) that

$$D_J = [\tilde{P}_J]_-^+ = \tilde{P}_J(\mathbf{k}, 0^+) = \frac{I}{k^2}\{e^{-i\mathbf{k}\cdot\mathbf{r}_A} - e^{-i\mathbf{k}\cdot\mathbf{r}_B}\}, \qquad \text{(A-4)}$$

where $[\ ]_-^+$ denotes the jump across the boundary $z = 0$.

Furthermore, according to equation (7), the horizontal projection $\tilde{\mathbf{H}}_h$ of the magnetic field is given by

$$\tilde{\mathbf{H}}_h = i(\mathbf{k} \times \hat{\mathbf{z}})\tilde{P}_J + i\mathbf{k}\tilde{P}_H'. \qquad \text{(A-5)}$$

Scalar multiplication with $-i\mathbf{k}$ gives

$$\tilde{P}_H' = -\frac{i\mathbf{k} \cdot \tilde{\mathbf{H}}_h}{k^2}, \qquad [\tilde{P}_H']_-^+ = -\frac{i\mathbf{k} \cdot [\tilde{\mathbf{H}}_h]_-^+}{k^2}. \qquad \text{(A-6)}$$

For the case of two point-current sources $+I$ and $-I$ at $\mathbf{r}_A$ and $\mathbf{r}_B$ connected by a straight cable along the unit vector $\hat{\mathbf{d}} = (\mathbf{r}_A - \mathbf{r}_B)/|\mathbf{r}_A - \mathbf{r}_B|$, the horizontal components of the magnetic field are, according to Biot-Savart's law,

$$\mathbf{H}_h(\mathbf{r}) = \frac{I(\hat{\mathbf{d}} \times \hat{\mathbf{z}})z}{4\pi} \int_{\mathbf{r}_B}^{\mathbf{r}_A} \frac{ds_0}{|\mathbf{r} - \mathbf{r}_0|^3}, \qquad \text{(A-7)}$$

with $\mathbf{r} = (x, y, z)$, $\mathbf{r}_0 = (x_0, y_0, 0)$, and $ds_0$ is the length of the line element. Transformation into the wavenumber domain gives

$$\tilde{\mathbf{H}}_h(\mathbf{k}, z) = \frac{I}{2}(\hat{\mathbf{d}} \times \hat{\mathbf{z}})\,\text{sign}(z) \int_{\mathbf{r}_B}^{\mathbf{r}_A} e^{-i\mathbf{k}\cdot\mathbf{r}_0 - k|z|}\,ds_0. \quad \text{(A-8)}$$

Thus

$$[\tilde{\mathbf{H}}_h(\mathbf{k}, z)]_-^+ = I(\hat{\mathbf{d}} \times \hat{\mathbf{z}}) \int_{\mathbf{r}_B}^{\mathbf{r}_A} e^{-i\mathbf{k}\cdot\mathbf{r}_0}\,ds_0$$

$$= I(\hat{\mathbf{d}} \times \hat{\mathbf{z}})\frac{e^{-i\mathbf{k}\cdot\mathbf{r}_A} - e^{-i\mathbf{k}\cdot\mathbf{r}_B}}{-i\mathbf{k} \cdot \hat{\mathbf{d}}}. \quad \text{(A-9)}$$

It then follows from equation (A-6) that

$$D_H = [\tilde{P}_H']_-^+ = I\frac{\mathbf{k} \cdot (\hat{\mathbf{d}} \times \hat{\mathbf{z}})}{k^2(\mathbf{k} \cdot \hat{\mathbf{d}})}\{e^{-i\mathbf{k}\cdot\mathbf{r}_A} - e^{-i\mathbf{k}\cdot\mathbf{r}_B}\}, \quad \text{(A-10)}$$

in agreement with equation (23), which also considers the limit $\mathbf{k} \cdot \hat{\mathbf{d}} = 0$.

## APPENDIX B

### STABLE COMPUTATION OF $\tilde{P}_J$ AND $\tilde{P}_H$

From equation (25), we infer that $-\alpha^-$ has a positive real part. Thus, the exponential terms with this exponent become unstable in numerical computations, especially for thick layers. On the other hand, $-\alpha^+$ has a negative real part. Thus, the exponential terms with this exponent are absolutely stable. Fortunately, there exists a relationship that admits a conversion between these terms. Isolating in the recurrence relation (33) positive and negative exponents, we obtain

$$\frac{\xi_\ell - B_{\ell+1}}{\xi_\ell - B_\ell}\,e^{-\gamma_\ell h_\ell} = \frac{\xi_\ell + B_{\ell+1}}{\xi_\ell + B_\ell}\,e^{+\gamma_\ell h_\ell}, \qquad \text{(B-1)}$$

or using equation (25),

$$\frac{\xi_\ell - B_{\ell+1}}{\xi_\ell - B_\ell}\,e^{-\alpha_\ell^+ h_\ell} = \frac{\xi_\ell + B_{\ell+1}}{\xi_\ell + B_\ell}\,e^{-\alpha_\ell^- h_\ell}. \qquad \text{(B-2)}$$

To calculate the integral in equations (38) and (39), we require $\tilde{T}_J(z)$, which according to equation (12), is in layer $\ell$ given by

$$\tilde{T}_J(z) = \frac{c_\ell k^2}{a_\ell}\tilde{P}_J(z) - \frac{b_\ell}{a_\ell}\tilde{P}_J'(z), \quad z_\ell < z < z_{\ell+1}. \quad \text{(B-3)}$$

First, the stable downward continuation of $\tilde{P}_J(z)$ and $\tilde{P}_J'(z)$ to subsequent layer boundaries yields for $1 \leq \ell \leq L - 1$

$$\frac{\tilde{P}_J(z_{\ell+1})}{\tilde{P}_J(z_\ell)} = \frac{\xi_\ell + B_\ell}{\xi_\ell + B_{\ell+1}}\,e^{-\alpha_\ell^+ h_\ell}, \qquad \text{(B-4)}$$

$$\frac{\tilde{P}_J'(z_{\ell+1}^-)}{\tilde{P}_J'(z_\ell^+)} = \frac{\xi_\ell + B_\ell}{\xi_\ell + B_{\ell+1}} \cdot \frac{\beta_\ell \xi_\ell + \gamma_\ell B_{\ell+1}}{\beta_\ell \xi_\ell + \gamma_\ell B_\ell}\,e^{-\alpha_\ell^+ h_\ell}, \quad \text{(B-5)}$$

$$\tilde{P}_J'(z_{\ell+1}^+) = \frac{1}{a_{\ell+1}d_{\ell+1}}\{a_{\ell+1}d_\ell \tilde{P}_J'(z_{\ell+1}^-)$$
$$+ (a_{\ell+1}e_\ell - a_\ell e_{\ell+1})\tilde{P}_J(z_{\ell+1})\}, \quad \text{(B-6)}$$

where $z_{\ell+1}^-$ lies in layer $\ell$ and $z_{\ell+1}^+$ in layer $\ell+1$. The last equation has been obtained by the fourth condition of equation (19). The variation in layer $\ell$, $z_\ell < z < z_{\ell+1}$, is

$$\frac{\tilde{P}_J(z)}{\tilde{P}_J(z_\ell)} = \frac{\xi_\ell + B_\ell}{\xi_\ell + B_{\ell+1}} \cdot \frac{(\xi_\ell + B_{\ell+1}) e^{-\alpha_\ell^+ (z-z_\ell)} + (\xi_\ell - B_{\ell+1}) e^{-\alpha_\ell^+ h_\ell + \alpha_\ell^- (z_{\ell+1}-z)}}{2\xi_\ell}, \tag{B-7}$$

$$\frac{\tilde{P}_J'(z)}{\tilde{P}_J'(z_\ell^+)} = \frac{\xi_\ell + B_\ell}{\xi_\ell + B_{\ell+1}} \cdot \frac{\alpha_\ell^+ (\xi_\ell + B_{\ell+1}) e^{-\alpha_\ell^+ (z-z_\ell)} + \alpha_\ell^- (\xi_\ell - B_{\ell+1}) e^{-\alpha_\ell^+ h_\ell + \alpha_\ell^- (z_{\ell+1}-z)}}{2(\beta_\ell \xi_\ell + \gamma_\ell B_\ell)}. \tag{B-8}$$

Finally, in layer $L$, the fields vary as

$$\frac{\tilde{P}_J(z)}{\tilde{P}_J(z_L)} = \frac{\tilde{P}_J'(z)}{\tilde{P}_J'(z_L^+)} = e^{-\alpha_L^+ (z-z_L)}. \tag{B-9}$$

The equations given above admit a stable computation of $\tilde{\mathbf{J}}$ and $\tilde{\mathbf{E}}$ at points inside the earth. All exponents have a negative real part.

For the computation of $\tilde{\mathbf{H}}$, the integral in equations (38) and (39) can be written as

$$\int_0^\infty \tilde{T}_J(z) e^{-kz} \, dz = I_1 + I_2 + I_3 + I_4, \tag{B-10}$$

where

$$I_1 = +\sum_{\ell=1}^{L-1} \frac{c_\ell k^2 \tilde{P}_J(z_\ell)}{2a_\ell \xi_\ell} \cdot \frac{\xi_\ell + B_\ell}{\xi_\ell + B_{\ell+1}}$$
$$\cdot \left\{ \frac{\xi_\ell + B_{\ell+1}}{k + \alpha_\ell^+} (e^{-kz_\ell} - e^{-kz_{\ell+1} - \alpha_\ell^+ h_\ell}) \right.$$

$$\left. + \frac{\xi_\ell - B_{\ell+1}}{k + \alpha_\ell^-} (e^{-kz_\ell - 2\gamma_\ell h_\ell} - e^{-kz_{\ell+1} - \alpha_\ell^+ h_\ell}) \right\}, \tag{B-11}$$

$$I_2 = -\sum_{\ell=1}^{L-1} \frac{b_\ell \tilde{P}_J'(z_\ell^+)}{2a_\ell(\beta_\ell \xi_\ell + \gamma_\ell B_\ell)} \cdot \frac{\xi_\ell + B_\ell}{\xi_\ell + B_{\ell+1}}$$

$$\cdot \left\{ \frac{\alpha_\ell^+ (\xi_\ell + B_{\ell+1})}{k + \alpha_\ell^+} (e^{-kz_\ell} - e^{-kz_{\ell+1} - \alpha_\ell^+ h_\ell}) \right.$$

$$\left. + \frac{\alpha_\ell^- (\xi_\ell - B_{\ell+1})}{k + \alpha_\ell^-} (e^{-kz_\ell - 2\gamma_\ell h_\ell} - e^{-kz_{\ell+1} - \alpha_\ell^+ h_\ell}) \right\}, \tag{B-12}$$

$$I_3 = +\frac{c_L k^2 \tilde{P}_J(z_L)}{a_L(k + \alpha_L^+)} e^{-kz_L}, \qquad I_4 = -\frac{b_L \tilde{P}_J'(z_L^+)}{a_L(k + \alpha_L^+)} e^{-kz_L}. \tag{B-13}$$